Mobility of Fluorobenzyl Alcohols Bound to Liver Alcohol Dehydrogenases as Determined by NMR and X-ray Crystallographic Studies[†,‡]

Jon K. Rubach and Bryce V. Plapp*

Department of Biochemistry, The University of Iowa, Iowa City, Iowa 52242

Received August 6, 2002; Revised Manuscript Received October 31, 2002

ABSTRACT: The relationship between substrate mobility and catalysis was studied with wild-type and Phe93Ala (F93A) horse liver alcohol dehydrogenase (ADH). Wild-type ADH binds 2,3,4,5,6-pentafluorobenzyl alcohol in one position as shown by X-ray results, and ^{19}F NMR shows five resonances for the fluorines of the bound alcohol. The two *meta*-fluorines exchange positions with a rate constant of about 4 s^{-1}, indicating that mobility (ring flipping) of the benzyl alcohol is relatively restricted. The wild-type enzyme binds 2,3-difluorobenzyl alcohol in two alternative conformations that are related by a ring flip and a small translation of the fluorinated benzene ring, and the ^{19}F NMR spectrum shows three resonances for the two bound fluorines, consistent with the two orientations. Phe-93 interacts with the bound benzyl alcohols, and the F93A substitution decreases the rate constants for hydride transfer for benzyl alcohol oxidation and benzaldehyde reduction by 7.4- and 130-fold, respectively. The structure of F93A ADH crystallized with NAD^+ and 2,3,4,5,6-pentafluorobenzyl alcohol is similar to the structure of the wild-type enzyme complex except that the pentafluorobenzyl alcohol is not found in one position. The ^{19}F NMR spectrum of the F93A ADH−NAD^+−pentafluorobenzyl alcohol complex shows three resonances for the bound fluorines. Line shape analysis of the spectrum suggests the bound pentafluorobenzyl ring undergoes rapid ring-flipping at about 20 000 s^{-1}. The F93A substitution greatly increases the mobility of the benzyl alcohol but modestly and differentially decreases the probability that the substrate is preorganized for hydride transfer.

Theories of enzyme catalysis invoking three point attachment for stereoselectivity (*1*), ground-state destabilization (*2*), or transition state stabilization (*3*) imply that substrates are firmly bound to enzyme active sites. However, examination of motions of substrates or inhibitors bound to enzyme active sites show the bound molecules can have significant mobility (*4*−*10*). The relationship between the dynamics of bound substrates and the rate of the chemical step of the catalyzed reaction is not well understood. Substrate motions are considered to be important for the preorganization that facilitates catalysis (*11*−*14*). Preorganization involves the appropriate arrangement of the protein and the substrates so that the chemical environment is primed for the reaction. Protein and substrate dynamics are involved in the alcohol dehydrogenase reaction, which proceeds with hydrogen tunneling (*15*−*22*), but how motions facilitate catalysis is not known. Studies on the mobility of enzyme-bound substrates or inhibitors are required to understand how the dynamics at the active site affect catalysis.

2,3,4,5,6-Pentafluorobenzyl alcohol, 2,4-difluorobenzyl alcohol, and 2,3-difluorobenzyl alcohol are close analogues of benzyl alcohol and good inhibitors of horse liver alcohol dehydrogenase. X-ray crystallography shows that pentafluorobenzyl alcohol binds in a single conformation in the substrate binding pocket, in a mode that appears poised for hydride transfer (*23*). The fluorinated alcohol interacts with several amino acid residues, including Phe-93, and rotation of the benzene ring would require movement of several residues. Since the rotation requires the local changes in protein conformation, the rotation of the phenyl rings of inhibitors bound to enzymes can define the time scale of protein motions at the active site (*24*).

To elucidate the roles of substrate motions in catalysis, we determined the effects of the F93A[1] substitution on the rates of catalysis and examined the binding of fluorinated benzyl alcohols to wild-type and F93A alcohol dehydrogenases using ^{19}F NMR and X-ray crystallography. The results provide quantitative information on the relationship between substrate mobility and the chemical step of catalysis.

EXPERIMENTAL PROCEDURES

Materials. Wild-type crystalline horse liver alcohol dehydrogenase (EE isoenzyme), LiNAD$^+$, and Na_2NADH were purchased from Roche Molecular Biochemicals. 2,3,4,5,6-

[†] This work was supported NIH Grants T32 GMO8365 and AA00279.

[‡] The X-ray coordinates and structure factors have been deposited in the RCSB Protein Data Bank with the entry names 1MGO for the F93A enzyme crystallized with NAD^+ and 2,3,4,5,6-pentafluorobenzyl alcohol and 1MG0 for the wild-type enzyme complexed with NAD^+ and 2,3-difluorobenzyl alcohol.

* Corresponding author. E-mail: bv-plapp@uiowa.edu; phone: 319-335-7909; fax: 319-335-9570.

[1] Abbreviations: ADH, alcohol dehydrogenase; PFB, 2,3,4,5,6-pentafluorobenzyl alcohol; 2,3-DFB, 2,3-difluorobenzyl alcohol; 2,4-DFB, 2,4-difluorobenzyl alcohol; F93A, substitution of Phe-93 with Ala; rmsd, root-mean-square deviation; t_m, mixing time; NOE, nuclear Overhauser effect.

10.1021/bi026581h CCC: $22.00
Published on Web 12/03/2002

Pentafluorobenzyl alcohol (98%), 2,4-difluorobenzyl alcohol (99%), and 2,3-difluorobenzyl alcohol (94%) were purchased from Aldrich. Benzyl alcohol-α,α-d_2 (98.6% D) was from MSD Isotopes. Deuterium oxide (99.9% D) was purchased from Aldrich. The trifluoroacetic acid was from Pierce. (4*R*)[4-^{2}H]NADD was prepared from NAD^+ and ethanol-d_6 (Aldrich, 99+% D) with yeast alcohol dehydrogenase (*25*) and purified on a DEAE-Sepharose column developed with a linear gradient of 10−250 mM sodium phosphate buffer, pH 8. Benzyl alcohol and benzaldehyde were redistilled. The F93A enzyme was expressed in an *Escherichia coli* XL1-Blue strain containing the plasmid pBPP/F93A (*26*), and purified according to the published procedure (*27*). The F93A enzyme was judged to be more than 95% pure as determined by polyacrylamide gel electrophoresis in the presence of sodium dodecyl sulfate.

Kinetic Studies. The buffer was 33 mM sodium phosphate and 0.25 mM EDTA, pH 8, at 25 °C. Coenzyme concentrations were determined by absorbance at 260 or 340 nm. The concentration of enzyme active sites (N, normality) was determined by titration with NAD^+ in the presence of pyrazole (*28*). Enzyme activity was determined on a Cary 118C spectrophotometer or an SLM 4800C fluorimeter (λ_{ex} = 340 nm, λ_{em} = 460), with computer fitting of the progress curves to obtain the initial velocities. The isotope effects on the initial velocities for benzyl alcohol oxidation were determined by measuring the initial velocities at a fixed concentration of 2 mM NAD^+ with varied concentrations of protio and deuterio benzyl alcohol. The isotope effects for benzaldehyde reduction were obtained by varying both the substrate and coenzyme concentrations, and the data were fitted to the equation for a sequential bi reaction. The steady-state kinetic data were fitted using Cleland's programs (*29*).

A BioLogic SFM3 stopped-flow instrument (dead time of 2.4 ms) was used to study the transient kinetics, and the BioKine software was used for data analysis. The transient oxidation reactions were studied with 10 μN enzyme, 2 mM NAD^+, and 10−240 μM benzyl alcohol or 33−400 μM benzyl alcohol-α,α-d_2. The reduction was studied with 10 μN enzyme with 50 μM NADH and 40−300 μM benzaldehyde or 100 μM NADH or 100 μM NADD and 50−5300 μM benzaldehyde. An extinction coefficient of 5500 M^{-1} cm^{-1} at 328 nm was used for the difference in absorption of NADH and NAD^+ bound to the enzyme and its complexes (*30*). Values for the microscopic rate constants were estimated by progress curve analysis using the kinetic simulation program, KINSIM, and the automatic fitting routine, FITSIM (*31*). An extinction coefficient of 26 M^{-1} cm^{-1} at 328 nm for the absorption of benzaldehyde was used for the simulation and fitting of the benzaldehyde reduction traces. Twenty progress curves, 9 for benzyl alcohol oxidation and 11 for benzaldehyde reduction, were used for fitting.

Transient kinetics were also used to determine the rate constant for dissociation of 2,3,4,5,6-pentafluorobenzyl alcohol from the wild-type enzyme−NAD^+−pentafluorobenzyl alcohol ternary complex, by trapping the E−NAD^+ complex with pyrazole. The enzyme−NAD^+−pyrazole complex absorbs at 294 nm (*28*). At saturating concentrations of pyrazole the formation of the E−NAD^+−pyrazole complex is limited by the dissociation of pentafluorobenzyl alcohol. The rate constants were determined by mixing a solution containing 20 μN enzyme, 2 mM NAD^+, and 100 μM pentafluorobenzyl alcohol with an equal volume of 3−60 mM pyrazole and 2 mM NAD^+, while measuring the increase of absorbance at 294. The progress curves were fitted to an equation that describes a first-order process. The observed rate constants at the varied concentrations of pyrazole were fitted using the HYPER program (*29*) to obtain the rate constant for the dissociation of pentafluorobenzyl alcohol.

X-ray Crystallography. The wild-type horse liver alcohol dehydrogenase used for the crystallography was recrystallized in 10 mM sodium phosphate buffer, pH 7.0, with 10% ethanol. These crystals were dissolved in a buffer containing about 0.5 M KCl and dialyzed against 50 mM ammonium *N*-[tris(hydroxymethyl)methyl]-2-aminoethanesulfonate buffer, 0.25 mM EDTA, pH 6.7 (measured at 25 °C) until the KCl and ethanol were removed. The enzyme solution was clarified by centrifugation. The crystals of the 2,3-difluorobenzyl alcohol ternary complex were produced by dialysis of 10 mg/mL enzyme against 11% 2-methyl-2,4-pentanediol in 50 mM ammonium *N*-[tris(hydroxymethyl)methyl]-2-aminoethanesulfonate buffer, 0.25 mM EDTA, pH 6.7, with 1 mM NAD^+ and 17 mM 2,3-difluorobenzyl alcohol. The final concentration of 2-methyl-2,4-pentanediol was raised to 25%. The crystals of the F93A enzyme−NAD^+−2,3,4,5,6-pentafluorobenzyl alcohol ternary complex were produced by dialysis of 26 mg/mL enzyme against 13% 2-methyl-2,4-pentanediol in 50 mM ammonium *N*-[tris(hydroxymethyl)methyl]-2-aminoethanesulfonate buffer, 0.25 mM EDTA, pH 6.7 (measured at 25 °C), with 20 mM NAD^+ and 100 mM pentafluorobenzyl alcohol. The final concentration of 2-methyl-2,4-pentanediol was raised to 20%.

The data for the 2,3-difluorobenzyl alcohol ternary complex were collected at 100 K with an R-Axis IV++ mounted on a rotating anode generator. Two data sets for the F93A enzyme−NAD^+−pentafluorobenzyl alcohol ternary complex were collected using the same crystal and were merged during processing. A low-resolution data set (20−1.6 Å) was collected with an R-Axis IV++ detector and the high-resolution data set (1.6−1.2 Å) was collected at the IMCA-CAT beam line at the Advanced Photon Source.

The data sets for the wild-type and F93A enzyme complexes were processed using d*TREK (Molecular Structure Corp.). The structures were solved by molecular replacement using AMORE (*32*) and the coordinates for the refined wild-type ADH−NAD^+-2,3,4,5,6-pentafluorobenzyl alcohol complex (1hld) as a model (*23*). For the molecular replacement the catalytic domains (residues 1−175, 319−374) and coenzyme binding domains (residues 176−318) were treated independently of each other. The structures were refined by cycles of restrained refinement with REFMAC (*33*) and model building with the program *O* (*34*). The NAD^+ and fluorinated alcohols were not included in the initial refinement of the models. The F93A substitution was made in the model only after clear negative density for the phenyl ring appeared in the $|F_o-F_c|$ map. The structures were checked using WHATIF (*35*) and PROCHECK (*36*).

^{19}F NMR Spectroscopy. For the wild-type ADH ternary complexes, 100 mg of crystalline horse liver ADH from Roche was dissolved in 2 mL of 1 mM sodium phosphate, 0.1 M sodium sulfate buffer, pH 8, and about 0.5 M KCl. It was then dialyzed against 1 mM sodium phosphate, 0.1 M sodium sulfate buffer, pH 8, until the KCl was removed.

Table 1. Steady State Kinetic Constants with Benzyl Alcohol and Benzaldehyde for Recombinant Wild-Type and F93A Enzymes[a]

kinetic constant	rADH[b]	F93A ADH
K_a (μM)	3.7	4.6
K_b (μM)	23	18
K_p (μM)	30	1090
K_q (μM)	1.7	0.26
K_{ia} (μM)	31	44[c]
K_{iq} (μM)	0.4	0.036[c]
V_1 (s^{-1})	2.2	0.31
V_2 (s^{-1})	22	2.0
V_1/K_b ($mM^{-1}\,s^{-1}$)	96	18
V_2/K_p ($mM^{-1}\,s^{-1}$)	700	1.8
K_{eq} (pM)[d]	40	70
turnover number (s^{-1})[e]	1.1	0.24
K_i pentafluorobenzyl alcohol (μM)	3.0	51[c]

[a] Kinetic constants were determined at 25 °C in 33 mM sodium phosphate and 0.25 mM EDTA buffer, pH 8.0. K_a, K_b, K_p, K_q are the Michaelis constants for NAD^+, benzyl alcohol, benzaldehyde, and NADH, respectively. K_{ia} and K_{iq} are the inhibition constants for NAD^+ and NADH, respectively. V_1 is the turnover number for benzyl alcohol oxidation, and V_2 is the turnover number for benzaldehyde reduction. The standard errors of the fits were < 25%. [b] Recombinant wild-type enzyme from ref *22*. [c] From ref *26*. [d] K_{eq} is the Haldane relationship calculated from $V_1K_pK_{iq}[H^+]/V_2K_bK_{ia}$. Values for the equilibrium constant have been estimated to be 35−70 pM (*51*−*53*). [e] Turnover number determined in a standard enzyme assay at 25 °C (*54*), based on titration of active sites.

The enzyme solution was clarified by centrifugation and assayed for activity. Deuterium oxide was added to make the solution 10% D_2O. The sample was concentrated to a volume of 0.5 mL using a Millipore centrifugal filter unit. Fluorinated benzyl alcohol, $LiNAD^+$ and trifluoroacetic acid (titrated to pH 7.3) were added to the enzyme solution and the sample volume was adjusted to 0.6 mL by addition of buffer containing 10% D_2O. The F93A ADH−NAD^+−pentafluorobenzyl alcohol sample was prepared using the same procedure except the purified enzyme was concentrated to 10 mg/mL before dialysis against the 1 mM sodium phosphate, 0.1 M sodium sulfate buffer (pH 8). The 1D fluorine ^{19}F NMR spectra were collected with a 500 MHz Varian spectrometer. The 2D ^{19}F,^{19}F-EXSY NMR spectra (*37*) were collected with a 300 MHz Bruker spectrometer, using mixing times of 25−200 ms. All samples contained 10% D_2O for the transmitter lock and 50 μM trifluoroacetic acid for chemical shift reference. T_1 values were determined by the inversion−recovery method (*38*), and T_2 was calculated from the line width of the peak. The program Mexico (*39*) was used to fit the line shape of the −83.9 ppm peak in the spectrum of the F93A ADH−NAD^+−pentafluorobenzyl alcohol ternary complex.

RESULTS

Kinetics of F93A ADH. Initial velocity data for the oxidation of benzyl alcohol and reduction of benzaldehyde, with systematically varied concentrations of coenzyme and substrate, were collected for the F93A enzyme and fit to the equation for a sequential bi reaction (Table 1). The F93A substitution significantly affects the kinetic constants, increasing affinity for NADH by 10-fold, as measured by the inhibition constant, and decreasing the turnover numbers (V_1 and V_2) for the oxidation and reduction reactions, by about 10-fold (Table 1). The increase of the isotope effects on V_2 and V_2/K_p to essentially the same value (Table 2) suggests that hydride transfer has become more rate limiting for benzaldehyde reduction.

Table 2. Kinetic Isotope Effects and Rate Constants for the Oxidation of Benzyl Alcohol and Reduction of Benzaldehyde by the Wild-Type and F93A Enzymes[a]

kinetic parameter	wild-type ADH	F93A ADH
$^DV_1$[b]	1.4 ± 0.1[c]	1.1 ± 0.1
$^DV_1/K_b$[b]	1.6 ± 0.5[c]	2.5 ± 0.4
$^DV_2$[b]	1.1 ± 0.1[c]	2.9 ± 0.2
$^DV_2/K_p$[b]	1.6 ± 0.5[c]	3.2 ± 0.2
$k_{max,\ oxidation}$ (s^{-1})[d]	24 ± 4[e]	3.3 ± 0.6
$k_{max,\ reduction}$ (s^{-1})[d]	320 ± 50[e]	2.2 ± 0.2
$^Dk_{max,\ oxidation}$[b]	3.6 ± 0.5[e]	4 ± 1
$^Dk_{max,\ reduction}$[b]	1.9 ± 0.3[e]	3.4 ± 0.2

[a] Experiments were performed at 25 °C in 33 mM sodium phosphate and 0.25 mM EDTA buffer, pH 8. [b] The superscript D represents the ratio of kinetic constants with protio and deuterio substrates. [c] From ref *55*. [d] Maximum rate constant for the transient oxidation of benzyl alcohol (20−250 μM) at a fixed concentration of 2 mM NAD^+, or benzaldehyde (0.05−5.3 mM) at a fixed concentration of 100 μM NADH. The maximum rate constant was determined by fitting the observed rate constants with the program HYPER (*29*). [e] From ref *40*.

The transient kinetics were studied to determine the effects of the F93A substitution on the rate constants for each step in the mechanism. The rate constants for the transient coenzyme binding reactions were determined previously (*26*). The transient reaction for the oxidation of benzyl alcohol catalyzed by the F93A enzyme has an initial exponential "burst" phase controlled by hydride transfer, followed by a steady-state phase controlled by coenzyme release. The reaction progress curves are similar to those for the transient oxidation of alcohols by the wild-type enzyme (*40*). With the F93A enzyme the rate constant for the burst phase at saturating concentrations of benzyl alcohol ($k_{max,\ oxidation}$) is 7-fold lower than the k_{max} for the wild-type enzyme (Table 2). The substrate isotope effect on the k_{max} for benzyl alcohol oxidation ($^Dk_{max,\ oxidation}$) is similar for both enzymes.

Transient reduction of benzaldehyde by the F93A enzyme differs from the wild-type enzyme in that it lacks an exponential burst phase. The k_{max} of 2.2 s^{-1} for hydride transfer to benzaldehyde for the F93A enzyme is decreased 145-fold from the rate constant of 320 s^{-1} observed with the wild-type enzyme (Table 2). The k_{max} for benzaldehyde reduction by the F93A enzyme has almost the same value as V_2, the k_{cat} for benzaldehyde reduction under steady-state conditions. The kinetic isotope effects are also similar for both the transient and steady-state experiments (Table 2). This suggests that the hydride transfer step, not the coenzyme release step, is rate limiting for benzaldehyde reduction by the F93A enzyme.

The microscopic rate constants for benzyl alcohol oxidation and benzaldehyde reduction were estimated from the simulation and fitting of the transient data by KINSIM/FITSIM (Table 3). Even though the rate constant for hydride transfer (k_3) has decreased 7-fold for benzyl alcohol oxidation with the F93A enzyme, the rate constant for the release of NADH (k_5) has also decreased and remains the rate-limiting step in benzyl alcohol oxidation (Table 3). Due to the large decrease of the rate constant for hydride transfer to benzaldehyde (k_{-3}), hydride transfer is limiting for benzaldehyde reduction catalyzed by the F93A enzyme, in contrast to the

Table 3. Estimated Rate Constants for the Oxidation of Benzyl Alcohol and Reduction of Benzaldehyde by Wild-Type and F93A Alcohol Dehydrogenases[a]

Reaction scheme:

$$E \underset{k_{-1}}{\overset{k_1}{\rightleftharpoons}} E\text{-}NAD^+ \underset{k_{-2}}{\overset{k_2}{\rightleftharpoons}} E\text{-}NAD^+\text{-}RCH_2OH$$

$$\underset{k_{-3}}{\overset{k_3}{\rightleftharpoons}} E\text{-}NADH\text{-}RCHO \underset{k_{-4}}{\overset{k_4}{\rightleftharpoons}} E\text{-}NADH \underset{k_{-5}}{\overset{k_5}{\rightleftharpoons}} E$$

rate constant	wild-type ADH[b]	F93A ADH
k_1 ($M^{-1}\,s^{-1}$)	1.2 ($\pm$ 0.12) $\times$ 10^6	1.9 ($\pm$ 0.18) $\times$ 10^6[c]
k_{-1} (s^{-1})	56 $\pm$ 6	220 $\pm$ 22[c]
k_2 ($M^{-1}\,s^{-1}$)	3.7 ($\pm$ 0.37) $\times$ 10^6	8.7 ($\pm$ 4.1) $\times$ 10^5
k_{-2} (s^{-1})	58 $\pm$ 5	110 $\pm$ 50
k_3 (s^{-1})	38 $\pm$ 3	5.1 $\pm$ 0.2
k_{-3} (s^{-1})	310 $\pm$ 30	2.3 $\pm$ 0.1
k_4 (s^{-1})	66 $\pm$ 6	360 $\pm$ 40
k_{-4} ($M^{-1}\,s^{-1}$)	8.3 ($\pm$ 0.83) $\times$ 10^5	2.5 ($\pm$ 0.29) $\times$ 10^5
k_5 (s^{-1})	5.5 $\pm$ 0.5	0.30 $\pm$ 0.03[c]
k_{-5} ($M^{-1}\,s^{-1}$)	1.1 ($\pm$ 0.11) $\times$ 10^7	1.3 ($\pm$ 0.13) $\times$ 10^7[c]

[a] Determined from the simulation and fitting of the progress curves for the transient oxidation of benzyl alcohol and the reduction of benzaldehyde at pH 8 and 25 °C. The data were fitted to the mechanism shown. The benzyl alcohol oxidation reactions used 10 μN F93A ADH, 2 mM NAD^+, and 20−240 μM benzyl alcohol. The benzaldehyde reduction reactions used 10 μN F93A ADH, 50 μM NADH and 40−5300 μM benzaldehyde or 10 μN F93A ADH, 50−5300 μM benzaldehyde and 100 μM NADH [b] From ref *40*. [c] From ref *26*.

reduction by the wild-type enzyme where the rate constant for NAD^+ dissociation is rate limiting (Table 3).

The rate constants can be used to estimate dissociation constants for the substrates. K_d for benzyl alcohol (k_{-2}/k_2) has increased from 0.016 mM for the wild-type enzyme to 0.13 mM for F93A ADH, and K_d for benzaldehyde (k_4/k_{-4}) has increased from 0.08 to 1.4 mM. The 8-fold decrease in affinity for benzyl alcohol is similar to the 17-fold decrease in affinity for pentafluorobenzyl alcohol (Table 1). The effects of the F93A substitution on the rate constants for hydride transfer appear to be related to the altered binding of the substrates.

Structure of the F93A ADH Crystallized in the Presence of NAD^+ and Pentafluorobenzyl Alcohol. The structure of the F93A enzyme was determined to evaluate the basis for the decreases in the affinities for the benzyl alcohols. The F93A enzyme crystallized with NAD^+ and pentafluorobenzyl alcohol in a triclinic space group with one dimer in the asymmetric unit. The X-ray data and refinement statistics are summarized in Table 4. The structure of the F93A complex is very similar to the structure of wild-type ADH complexed with NAD^+ and pentafluorobenzyl alcohol (*23*). The peptide backbone C_α atoms of the F93A and wild-type enzyme dimers superimpose well, with a rmsd of 0.24 Å. The NAD^+, the catalytic zinc and the proton relay system are in the same positions and conformations in the F93A and wild-type enzyme structures (*23*). The structure does not suggest how the F93A substitution affects affinity for NADH, but the structure of the binary enzyme−NADH complex could be different than the one with NAD^+.

The major differences between the F93A and wild-type enzyme structures are in the conformations of the leucine side chains at the active site, in particular, Leu-116 (Figure 1). This probably arises from the increased flexibility at the binding site due to the F93A substitution. The structure of the F93A enzyme was refined without including pentafluorobenzyl alcohol bound to the active site zinc. Electron density that could be due to the pentafluorobenzyl alcohol is present at the active sites, but it is ambiguous and does not allow for fitting of the alcohol in a single conformation. The substitution opens up the substrate binding site and allows the benzyl alcohol to bind in other conformations or undergo more large scale motions. The pentafluorobenzyl alcohol can be modeled in the same position as seen in the wild-type enzyme structure, as well as in a conformation that occupies the space created by the F93A substitution. In the final structure, the electron density in the active site of the B subunit was fitted with 2-methyl-2,4-pentanediol. However, the electron density could be due to pentafluorobenzyl alcohol bound in multiple conformations. The electron density at the active site of the A subunit is not adequately modeled by methylpentanediol and could also be due to pentafluorobenzyl alcohol bound in multiple conformations, which would include some in which the α-carbon is not in the correct orientation for hydride transfer.

Table 4. X-ray Data and Refinement Statistics for F93A and Wild-Type ADH Complexed with NAD^+ and Fluorobenzyl Alcohols

enzyme	F93A	wild-type
alcohol	pentafluorobenzyl	2,3-difluorobenzyl
PDB entry	1MGO	1MG0
space group	*P*1	$P2_1$
molecules per unit cell	1	2
cell dimensions, Å	44.1, 51.3, 93.5,	50.1, 180.3, 86.9
cell angles, deg	91.9, 103.0, 109.8	90.0, 105.9, 90.0
resolution range, Å	20.0−1.2	20.0−1.8
measured reflections: unique, total	199422, 455785	118298, 243387
completeness, % (outer shell)	86.6 (84.5)	88 (50)
R_{sym}, % (outer shell)[a]	7.3 (29.0)	4.0 (18.0)
mean $<I>/\sigma<I>$ (outer shell)	5.3 (1.5)	16 (3.1)
R_{value}, R_{free}, test %[b]	18.8, 21.0, 1.0	17.9, 21.4, 1.5
rsmd for bond distances[c]	0.019	0.012
rmsd for bond angles	1.84	1.29
water molecules per dimer	465	453

[a] $R_{sym} = (\Sigma|I - <I>|)/\Sigma<I>$, where I is the integrated intensity of a given reflection. [b] $R_{value} = (\Sigma||F_o| - k|F_c||)/\Sigma|F_o|$, where k is a scale factor. The R_{free} (*56*) values were calculated with the indicated percentage of reflections not used in the refinement. [c] Root-mean-square deviations (rmsd) from the ideal geometry of the final model.

The active sites should have bound pentafluorobenzyl alcohol because the inhibition constant for the pentafluorobenzyl alcohol is 51 μM, and the concentration of the alcohol used in the crystallization was 100 mM. Indeed, a pentafluorobenzyl alcohol molecule is located farther down in the substrate binding pocket near the sulfur of Met-306 in subunit A, but not in subunit B, and an additional pentafluorobenzyl alcohol molecule is bound in a small cleft between Pro-136 and His-138 on the surface of the B subunit. These pentafluorobenzyl alcohols were modeled with partial occupancies, suggesting low affinities, and their binding probably is due to the very high concentration of pentafluorobenzyl alcohol. The binding sites are distant from the coenzymes in the active sites and are not likely to be relevant to catalysis.

Structure of the Wild-Type ADH−NAD^+−2,3-Difluorobenzyl Alcohol Complex. The structure of the ADH−NAD^+−2,3-difluorobenzyl alcohol ternary complex was solved to determine if the enzyme could distinguish the hydrogens from the fluorines and bind the 2,3-substituted benzyl ring

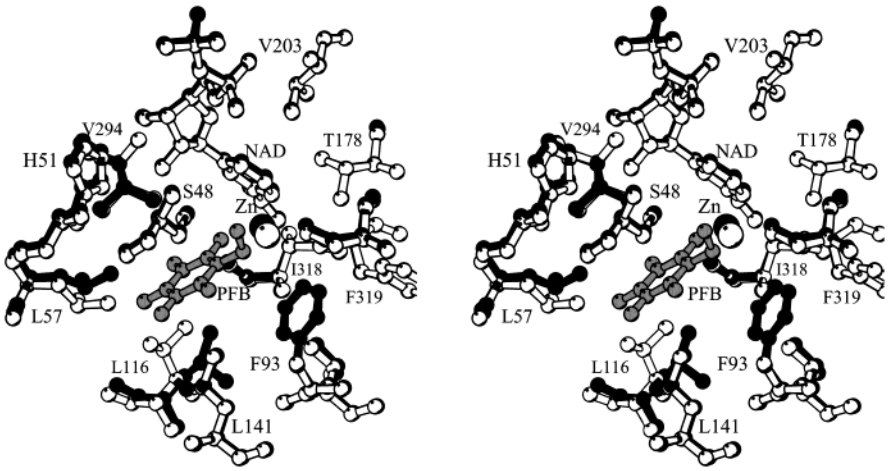

FIGURE 1: Structural comparison of the 2,3,4,5,6-pentafluorobenzyl alcohol ternary complexes with F93A and wild-type alcohol dehydrogenase. The coenzyme binding domains of the F93A (white, PDB entry 1MGO) and wild-type (black, PDB entry 1HLD) were superimposed using the program *O*. The 2,3,4,5,6-pentafluorobenzyl alcohol (PFB) of the wild-type ADH complex is shown in gray.

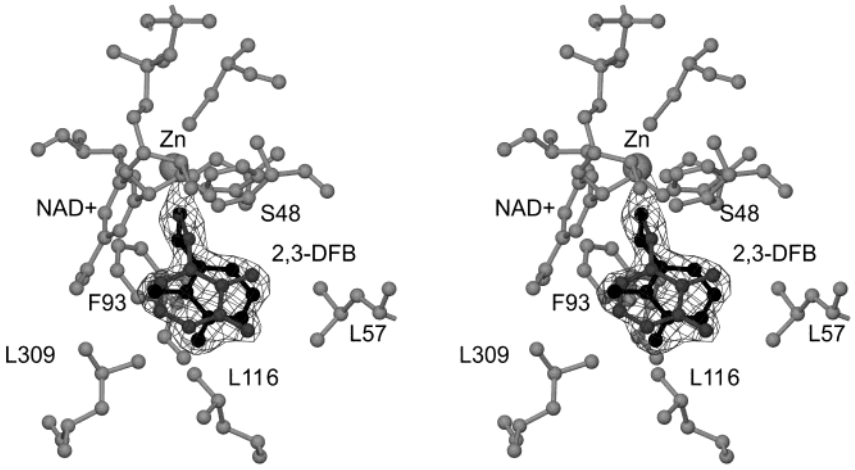

FIGURE 2: Alternative binding conformations of 2,3-difluorobenzyl alcohol at the active site of horse liver alcohol dehydrogenase. The final $2|F_o - F_c|$ electron density map covering the bound alcohols is shown (contoured at 1.0 σ).

in one conformation.[2] 2,3-Difluorobenzyl alcohol binds to the enzyme−NAD^+ complex, is a competitive inhibitor against alcohols and is unreactive as a substrate. The K_i for 2,3-difluorobenzyl alcohol is 6.5 ± 0.4 μM at pH 8, 25 °C. The 2,3-difluorobenzyl alcohol ternary complex crystallized in a monoclinic space group with two dimers in the asymmetric unit. The X-ray data and refinement statistics are summarized in Table 4.

Each of the four subunits has a "closed" conformation, similar to the structures of other ternary complexes (*23*, *41*−*43*). The NAD^+ is bound in the same position and interacts with the same residues as described previously (*23*). The electron density for the fluorinated benzyl ring of the 2,3-difluorobenzyl alcohol is best fit by two alternative conformations of the ring that are related by a 180° rotation about the C1 to C4 axis (ring flip) and a small translation (Figure 2). If the 2,3-difluorobenzyl alcohol is modeled in either one of the two conformations, significant positive density in the $|F_o-F_c|$ difference electron density maps is present for the atom positions for the other conformation. To determine the relative occupancies of the conformations, we assumed that the motions of the atoms in the two conformations are the same and should have the same temperature factors. This assumption was made because the values for the temperature factors and occupancies are highly correlated. Thus, the occupancies for the atoms of the 2,3-difluorobenzyl alcohol in the alternative conformations were adjusted during refinement so that the temperature factors would have similar values. The 2,3-difluorobenzyl rings at the active sites fit best with equal (0.5:0.5) occupancies. The difference electron density maps calculated with these occupancies showed no significant positive or negative contours. The peptide backbones and the side chain rotamers of the residues in the active sites of the four subunits superposition well. The only exception is that the side chain of Leu-116 in the D subunit has a slightly different rotamer conformation as compared to the other subunits.

The 2,3-difluorobenzyl alcohol conformers are slightly offset in the same plane as the ring, so the rings and methylene groups of the conformers do not overlap. In one of the conformations the pro-*R* hydrogen points toward the C4 of NAD^+ and is oriented for hydride transfer, but in the other conformation the *pro-R* hydrogen is pointed away from the nicotinamide ring. The two conformations of the 2,3-difluorobenzyl alcohol make different contacts with the

[2] With respect to the different positions for the binding of benzyl alcohols, we use "conformation" in the sense that the inhibitors have different orientations in the complexes.

Table 5. Contacts between Atoms of the 2,3-Difluorobenzyl Alcohol and the Enzyme and Coenzyme

conformation	atoms	distances (Å) to residue, atoms		
A or B	O1	2.6 Ser48 OG	3.1 NAD NC5	3.1 His67 NE2
A	C7	3.6 NAD NC4	3.7 Phe93 CZ	
A	C3	3.7 Leu116 CD1	3.8 Leu116 CD2	
A	C4	3.6 Leu57 CD1	3.6 Leu116 CD2	
A	C5	3.6 Leu57 CD2	3.7 Leu141 CD1	
A	C6	3.1 NAD NO7	3.2 NAD NC7	3.3 Ser48 CB
A	F2	2.9 NAD NC7	3.0 NAD NO7	3.1 NAD NC3
A	F3	3.4 Val294 CG2	3.5 Leu116 CD2	3.8 Leu309 CD2
B	C7	3.9 NAD NC4	4.0 Phe93 CZ	
B	C3	3.5 Leu116 CD1		
B	C4	3.8 Leu116 CD1	3.5 Leu294 CG2	
B	C5	3.5 NAD NO7	3.6 Ile318 CD1	3.7 Val294 CG2
B	C6	3.2 NAD NC3	3.3 NAD NO7	3.4 NAD NC7
B	F2	3.3 Ser48 CB	3.3 Leu57 CD2	3.8 Leu141 CD1
B	F3	3.1 Leu116 CD1	3.1 Leu57 CD1	3.5 Leu57 CD2

amino acid side chains in the active site (Table 5). The positions of the 2,3-difluorobenzyl rings probably differ because of the differences in the bond lengths and van der Waals radii for fluorine as compared to hydrogen. The length of an aromatic carbon−fluorine bond is 1.3 Å (*44*), and fluorine has a slightly elliptical van der Waals radius of 1.34 Å (*45*). An aromatic carbon−hydrogen bond has a length of 1.1 Å (*44*) and an aromatic hydrogen has a van der Waals radius of 1.0 Å (*46*). These differences make the van der Waals contact radius for the side of the benzene ring with the fluorines larger than that of the unsubstituted side and can account for the offset ring positions of the alternative conformations. The results show that binding of benzyl alcohol is flexible, which should affect the rates of catalysis.

^{19}F NMR Spectra of Fluorinated Benzyl Alcohols Bound to Wild-Type ADH. The 1D ^{19}F NMR spectrum of the 2,3-difluorobenzyl alcohol ternary complex shows three broadened peaks (Figure 3A and Table 6). The sharp peaks at −63.3 and −66.9 ppm are due to impurities. The peaks at −63.9 and −69.9 ppm include both bound and free resonances. The presence of three peaks for the bound species indicates that the 2,3-difluorobenzyl alcohol binds in more than one conformation, as shown by the X-ray results. The spectrum does not show significant temperature dependence between 4 and 43 °C (data not shown), which suggests the exchange between the bound conformations is not rapid. The ^{19}F, ^{19}F-EXSY NMR spectrum of the 2,3-difluorobenzyl alcohol complex (data not shown) shows cross-peaks between the peaks at −60.8 and −63.9 ppm in the 1D spectrum. The presence of cross-peaks suggest exchange is occurring between the two resonances. However, since one of the resonances results from both free and bound species it is not clear how much of the cross-peak intensity is due to exchange between the bound states and how much is due to the exchange between the bound and free states.

The 1D ^{19}F NMR spectrum of the 2,4-difluorobenzyl alcohol ternary complex also shows three broadened peaks for the bound inhibitor (Figure 3B and Table 6). The presence of three resonances for two bound fluorines suggests the inhibitor binds in more than one conformation. The peaks at −35.3 and −40.5 ppm in the spectrum of the 2,4-difluorobenzyl alcohol ternary complex include both bound and free resonances (Table 6). The sharp peaks at −32.3 and −35.4 ppm are due to impurities. The overlapping peaks

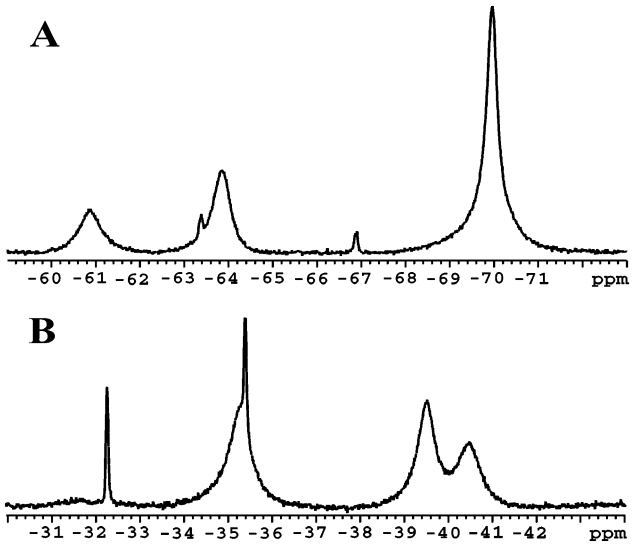

FIGURE 3: 1D ^{19}F NMR spectra of difluorobenzyl alcohol ternary complexes with wild-type alcohol dehydrogenase. (A) ADH−NAD$^+$−2,3-difluorobenzyl alcohol complex (bound *meta*-fluorine, −60.8 and −63.9 ppm; bound *ortho*-fluorine, −69.9 ppm). The sample contained 3.5 mN ADH, 3.8 mM NAD$^+$, 3.8 mM 2,3-difluorobenzyl alcohol. (B) ADH−NAD$^+$−2,4-difluorobenzyl alcohol complex (bound *para*-fluorine, −35.3 ppm; bound *ortho*-fluorine, −39.5 and −40.5 ppm). The sample contained 1.5 mN ADH, 1.5 mM NAD$^+$, 1.8 mM 2,4-difluorobenzyl alcohol.

Table 6. ^{19}F NMR Chemical Shifts for Fluorinated Benzyl Alcohols Free and Complexed to Alcohol Dehydrogenases[a]

	ortho		meta		para	
enzyme complex	free	bound	free	bound	free	bound
wild-type 2,3-DFB	−70.0	−69.9	−64.1	−60.8, −63.9		
wild-type 2,4-DFB	−40.3	−39.5, −40.5			−35.6	−35.3
wild-type PFB	−69.6	−66.2, −69.4	−87.4	−82.7, −85.9	−79.6	−81.3
F93A PFB	−69.6	−68.3	−87.4	−83.9	−79.6	−79.7

[a] Chemical shifts are in ppm and are referenced to trifluoroacetic acid.

for bound and free difluorobenzyl alcohol prevent determination of the relative occupancies of each conformation from the integrals of the peaks for the bound ligand and the rate of exchange between the bound species through 2D EXSY and saturation transfer experiments.

The spectrum of the ADH−NAD$^+$−2,3,4,5,6-pentafluorobenzyl alcohol ternary complex shows seven peaks (Figure 4A and Table 6). The peaks at −66.2 and −69.4 ppm are from the bound *ortho*-fluorines, but the peak at −69.4 ppm has both bound and free components. The T_1 values for the bound fluorine atoms are about 1.5 s at 25 °C. The line width of the peak at −85.9 ppm, corresponding to a bound *meta*-fluorine, is 106 Hz at 25 °C. The T_1 values for the unbound fluorines are slightly different from those of the bound fluorines, with a T_1 of 1.45 s for the unbound *ortho*- and *para*-fluorines and a T_1 of 1.8 s for the unbound *meta*-fluorine. The spectrum for the pentafluorobenzyl alcohol ternary complex does not show significant temperature dependence between 4 and 35 °C (data not shown), which suggests that exchange between the bound resonances is not rapid. The peaks slightly broaden as the temperature de-

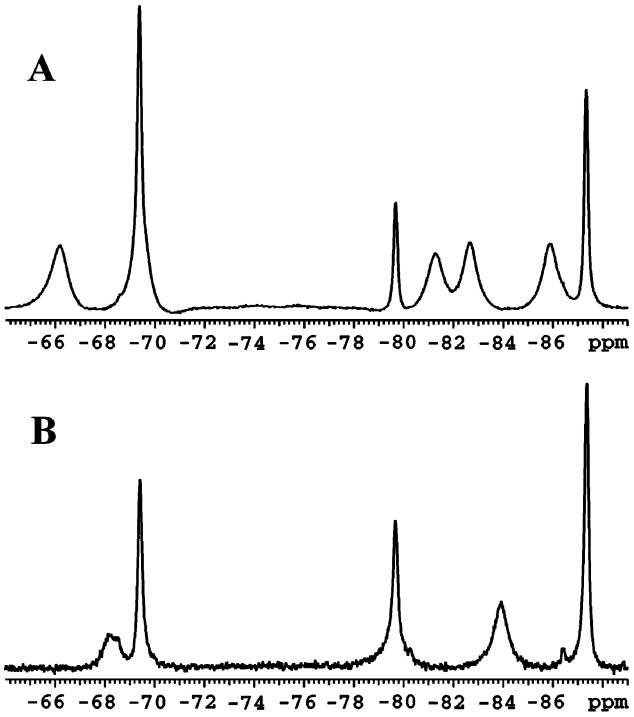

FIGURE 4: 1D ^{19}F NMR spectra of 2,3,4,5,6-pentafluorobenzyl alcohol ternary complexes with wild-type and F93A alcohol dehydrogenase. (A) Wild-type ADH−NAD^+−2,3,4,5,6-pentafluorobenzyl alcohol complex (bound *ortho*-fluorines, −66.2, −69.4 ppm; free *ortho*-fluorines, −69.6 ppm; bound *para*-fluorine, −81.3 ppm, free *para*-fluorine, −79.6 ppm; bound *meta*-fluorines, −82.7 and −85.9 ppm; free *meta*-fluorines, −87.4 ppm). The sample contained 2 mN ADH, 2 mM NAD^+ and 2.5 mM pentafluorobenzyl alcohol. (B) F93A ADH−NAD^+−2,3,4,5,6-pentafluorobenzyl alcohol complex (bound *ortho*-fluorines, −68.3 ppm; free *ortho*-fluorines, −69.6 ppm; free *para*-fluorine, −79.6 ppm; bound *para*-fluorine; −79.6 ppm, bound *meta*-fluorines, −83.9 ppm; free *meta*-fluorines, −87.4 ppm). The sample contained 0.68 mN F93A ADH, 0.7 mM NAD^+, 0.68 mM pentafluorobenzyl alcohol.

creases from 25 to 4 °C, which is likely due to changes in viscosity. The resonance at −85.9 ppm has a line width of 150 Hz at 4 °C. The chemical shift of the *meta*-peak at −82.7 shifts about 0.8 ppm over the 31 degree temperature range.

A saturation transfer experiment was used to measure the rate of exchange between the two *meta*-fluorine atoms of the enzyme-bound pentafluorobenzyl alcohol. The effect of increasing saturation of the peak at −89.5 ppm on the intensity of the peak at −82.7 ppm was measured and fitted to an equation based on a first-order decay equation (Figure 5A). Fitting the saturation transfer data for the peak at −82.7 ppm (bound *meta*-fluorine) yields an exchange rate of 1.9 s^{-1}. The data from the saturation transfer experiment show that there is not much magnetization transfer, only about 23%, between the peaks corresponding to the *meta*-fluorines of the bound alcohol during the saturation pulse. Even though the 0.15 s saturation pulse effectively removed the peak at −85.9 ppm, the other peaks in the spectrum were not severely affected (after the large effect of the saturation pulse on the intensity is accounted for).

The ^{19}F, ^{19}F-EXSY spectra of the wild-type ADH−NAD^+−2,3,4,5,6-pentafluorobenzyl alcohol ternary complex show several cross-peaks between the five enzyme-bound fluorines (Figure 6). The cross-peaks are due to the conformational exchange of the fluorines or the NOEs between the fluorines. A small portion of the volume of the *meta*-

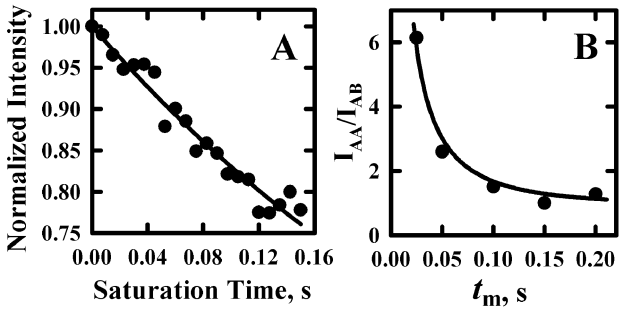

FIGURE 5: Exchange rates determined by saturation transfer and EXSY experiments. (A) Saturation transfer from the resonance at −85.9 ppm to the resonance at −82.7 ppm of the ^{19}F NMR spectrum for the wild-type ADH−NAD^+−2,3,4,5,6-pentafluorobenzyl alcohol complex. The fitted data give an observed exchange rate constant of 1.9 ± 0.1 s^{-1}. The peak at −85.9 ppm was saturated for increasing lengths of time, 0 to 0.15 s, in steps of 0.0075 s, and the effects of the saturation on the integral of the peak at −82.7 ppm was monitored. The measured integrals at each saturation time were normalized to the integral of the peak at −79.6 ppm. The normalized integrals (I) at time (t) were fitted to the equation: $I(t) = [k_{-1}/(1/T_1 + k_{-1})]\exp[(1/T_1 + k_{-1})t] + [1/T_1/(1/T_1 + k_{-1})]$ (*57*) using NONLIN (*58*). (B) The change in the ratio of the integral of the *meta*-fluorine peaks on the diagonal (I_{AA}) to the integral of the *meta*-fluorine cross-peaks (I_{AB}) with the mixing time of the pulse sequence (t_m). The fitted data give an observed rate constant of 6.9 ± 0.3 s^{-1}. The I_{AA}/I_{AB} at different t_m values was fitted to the equation: $I_{AA}/I_{AB} = \{[1 + \exp(-2kt_m)]\exp(-t_mR)\}/\{[1 - \exp(-2kt_m)]\exp(-t_mR)\}$ (*57*) using NONLIN (*58*). R ($1/T_1$) is equal to 0.76 s^{-1}.

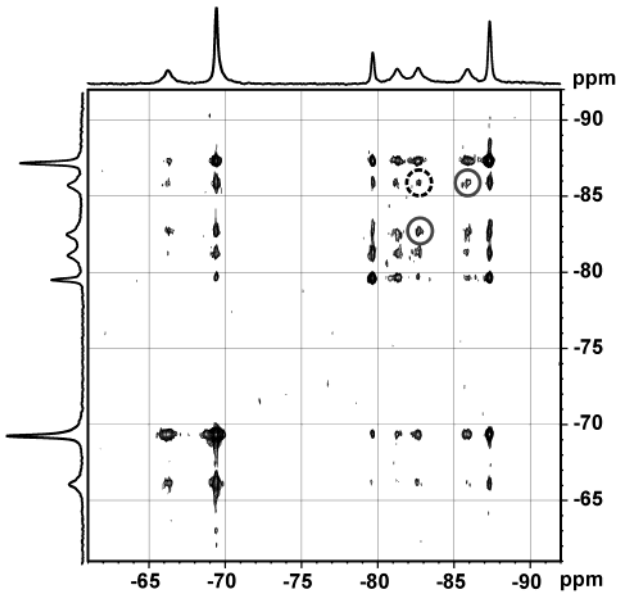

FIGURE 6: ^{19}F, ^{19}F-EXSY NMR spectrum of the wild-type ADH−NAD^+−2,3,4,5,6-pentafluorobenzyl alcohol complex. The sample contained 2 mN ADH, 2.2 mM NAD^+, and 2.5 mM 2,3,4,5,6-pentafluorobenzyl alcohol. The t_m for the spectrum was 150 ms. The peaks corresponding to the *meta*-fluorines are indicated by the gray circles. The cross-peak due to the exchange is indicated by the dashed circle.

fluorine cross-peak is due to the NOE between the two *meta*-fluorines, which are 4.7 Å from each other. This NOE contribution to the cross-peak should be the same as the NOE cross-peak between the *para*- and *ortho*-fluorines, which are the same distance from each other as the *meta*-fluorines but are not undergoing exchange. When the spectrum is collected with a t_m of 25 ms, the integrals for the cross-peaks of the *meta*-fluorines are six times larger than the integrals of the

cross-peaks of the *ortho*- and *para*-resonances. This suggests the cross-peaks of the two bound *meta*-fluorines have a significant contribution from the exchange that occurs as the enzyme-bound pentafluorobenzyl ring undergoes a 180° rotation. The peak integrals of the *meta*-fluorine cross-peaks and diagonal peaks at increasing t_m values were fitted to the equation shown in Figure 5 and give a rate constant of 6.9 $\pm$ 0.3 s^{-1} for the exchange (Figure 5B). The rate constant obtained from fitting the change in the integrals of the *meta*- and *para*-fluorine NOE cross-peaks to the same equation is 1.0 $\pm$ 0.2 s^{-1}. The rate due to the contribution of the NOE intensity to the cross-peak should be the same for the *meta*-fluorines as for the *para*- and *ortho*-fluorines and subtracting the rate of 1.0 s^{-1} from 6.9 s^{-1} gives 5.9 s^{-1} as the rate constant for exchange, i.e., ring flipping.

The rate constant for the dissociation of 2,3,4,5,6-pentafluorobenzyl alcohol from the wild-type ADH−NAD^+−2,3,4,5,6-pentafluorobenzyl alcohol ternary complex was determined by measuring the rate at which the wild-type ADH−NAD^+ complex is trapped by pyrazole, once the pentafluorobenzyl alcohol dissociates. At saturating concentrations of pyrazole, the rate constant for pentafluorobenzyl alcohol dissociation is 0.5 $\pm$ 0.1 s^{-1}. This rate constant is one-tenth the value of the constant calculated for ring flipping.

^{19}F NMR Spectrum of the F93A ADH−NAD^+−2,3,4,5,6-Pentafluorobenzyl Alcohol Ternary Complex. The ^{19}F NMR spectrum of the F93A ternary complex was examined to determine the effects of the substitution on the mobility of the bound pentafluorobenzyl alcohol. The spectrum for the fluorines of the pentafluorobenzyl alcohol bound to the F93A enzyme shows only two peaks, at −68.3 and −83.9 ppm, that are separated from the peaks of the free alcohol (Figure 4B and Table 6). The peak for the bound *ortho*-fluorines is at −68.3 ppm, which is approximately the average of the chemical shifts for the two *ortho*-fluorine peaks, −66.2 and −69.4 ppm, in the spectrum for the wild-type enzyme ternary complex (Figure 4A). The peak for the bound *meta*-fluorines at −83.9 ppm (Figure 4B) is approximately the average of the chemical shifts for the *meta*-fluorines in the spectrum of the wild-type enzyme ternary complex, −82.7 and −85.9 ppm (Figure 4A). The peak for the bound *para*-fluorine is at the same chemical shift as the peak for the free *para*-fluorine, −79.6 ppm. These results suggest the two separate peaks for the *ortho*- and *meta*-fluorines are averaged to a single peak due to "fast" flipping of the benzyl ring.

The spectrum for the F93A ADH pentafluorobenzyl alcohol ternary complex is temperature dependent. At 25 °C the peak at −83.9 ppm has a T_1 of 1.0 s and a line width of 258 Hz. At 5 °C the peak at −83.9 ppm has a T_1 of about 1 s and a line width of 320 Hz. This line width is corrected for contributions from changes in viscosity by subtracting the amount the line width has increased from 25 to 4 °C in the spectrum of the complex of wild-type enzyme with pentafluorobenzyl alcohol. For the F93A enzyme spectra, the peaks for the bound fluorines broaden into the baseline as the temperature decreases to 5 °C, but no other peaks appear. The enzyme is not sufficiently stable to examine the temperature dependence of the spectra above 25 °C. The lack of the two peaks for the bound *ortho*- and *meta*- fluorines and the broadening of the peaks at low temperatures suggest the resonances for the *ortho*- and *meta*-fluorines of the bound pentafluorobenzyl alcohol are averaged by "fast" exchange.

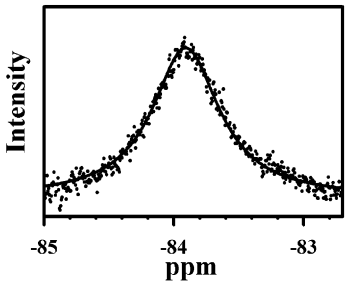

FIGURE 7: Exchange rate determined from line shape analysis of the ^{19}F NMR spectrum of the F93A ADH−NAD^+−pentafluorobenzyl alcohol ternary complex. The fitted data for the peak at −83.9 ppm give a rate constant for exchange of 20 000 s^{-1}. The program MEXICO (*39*) was used to fit the line shape. In the absence of exchange, the difference in chemical shift between the bound *meta*-fluorines of the F93A ADH−NAD^+−pentafluorobenzyl alcohol complex was assumed to be the same as for the wild-type enzyme complex at 25 °C (1516 Hz). The midpoint distance of the theoretical resonances in the absence of exchange was fixed at −83.9 ppm. We assumed the exchange was occurring through a two-site exchange model (*57*).

The line shape for the peak at −83.9 ppm was fit using the program Mexico. The −83.9 ppm resonance at 25 °C was best fit by an exchange rate constant of 20 000 s^{-1} (Figure 7). The difference in Hz between the peaks for the two *meta*-fluorines bound to the F93A enzyme, in the absence of exchange, was set at 1516 Hz (3.2 ppm). This was based on the difference in Hz between the *meta*-peaks of the wild-type enzyme complex, which are in slow exchange.

Using the value of 1516 Hz may be an incorrect assumption, but the chemical shift difference between the pairs of peaks for bound pentafluorobenzyl rings of inhibitors bound to enzymes have ranged from 2.3 ppm (*10*) to 6 or 8.5 ppm (*47*). The effect of removing the ring current of the phenyl ring on the spectrum is not likely to be large. The fluorines of pentafluorobenzyl alcohol bound to wild-type enzyme are not in van der Waals contact with the Phe-93 side chain, and the contribution of ring currents on the fluorine chemical shift are thought to be rather small compared to the effect of short-range electronic effects of nearby carbonyl and amide groups (*48*). With dihydrofolate reductase, the effect of a ring current on the fluorine of 6-fluorotryptophan that is within van der Waals contact of an indole side chain of another tryptophan residue was calculated to be at most −0.4 to 0.47 ppm (*48*). Fitting the line shape using 916 Hz (1.95 ppm) as the difference gives a rate constant of 7300 s^{-1}, which is still significantly faster than the observed rate constants of 1.9 and 5.9 s^{-1} that were determined with the wild-type enzyme complex.

DISCUSSION

The central issue addressed in this work is the relationship between substrate motions and catalytic activity. The involvement of substrate motion in catalysis by alcohol dehydrogenase has been inferred from the involvement of hydrogen tunneling in the reaction (*15*−*22*). Moreover, since the rate constant for hydride transfer increases as the number of carbons in the alcohol substrate increases (*40*), it appears the reaction is facilitated by a higher probability of a preorganized conformation.

The studies on the fluorinated alcohols bound to wild-type alcohol dehydrogenase show the alcohols are mobile when bound at the active site. The crystallographic and NMR studies on the ADH−NAD^+−2,3-difluorobenzyl alcohol

ternary complex suggest the 2,3-difluorobenzyl alcohol binds in at least two different conformations (Figures 2 and 3), which are likely to interconvert. Analysis of the saturation transfer and ^{19}F, ^{19}F-EXSY data for the ADH−NAD^+−2,3,4,5,6-pentafluorobenzyl ternary complex suggest that the pentafluorobenzyl ring of the enzyme-bound inhibitor rotates (flips) with a rate constant of about 4 s^{-1}, the average of 1.9 and 5.9 s^{-1} (Figures 4 and 5). The rotation of the bound pentafluorobenzyl ring requires the movement of several active site residues. Therefore, the rate constant of 4 s^{-1} for ring flipping provides a time scale for motions of amino acid residues at the active site.

It is likely that the bound alcohols have motions on a faster time scale. The structure of the crystalline 2,3-difluorobenzyl alcohol ternary complex shows the α-carbon of the alcohol, from which the hydride is transferred, can access an alternative conformation in which the *pro-R* hydrogen is not in-line for transfer to the nicotinamide ring (Figure 2). This conformation is also observed for *para*-bromobenzyl alcohol bound at the active site (*23*, *49*). The observation of these different α-carbon positions in the crystal structures suggests the benzyl alcohol accesses them when the enzyme is in solution.

The role of Phe-93 in substrate binding was investigated by kinetic, crystallographic and NMR studies on the F93A substituted enzyme. Phe-93 is located in the substrate binding pocket and interacts with the methylene (α-carbon) of the bound pentafluorobenzyl alcohol (Figure 1) or 2,3-difluorobenzyl alcohol (Figure 2). The distance between the α-carbon of the pentafluorobenzyl alcohol and the CZ of Phe-93 is 3.5 Å. The presence of the Phe-93 side chain restricts the binding conformations of the α- and *β*-carbons in the substrates, which is thought to lead to the binding of substrates in an orientation that facilitates hydride transfer of the pro-*R* hydrogen (*49*). We expected the F93A substitution to decrease the affinity for the pentafluorobenzyl alcohol, benzyl alcohol and benzaldehyde. However, the increased affinity for NADH and differential effects on hydride transfer were not expected. The rate constants for hydride transfer catalyzed by the F93A enzyme, as compared to the wild-type enzyme, decrease by 7.4-fold for benzyl alcohol oxidation (k_3) to a value of 5.1 s^{-1} and by 130-fold for benzaldehyde reduction (k_{-3}) to a value of 2.3 s^{-1} (Table 3). In addition, hydride transfer is now the rate-limiting step for benzaldehyde reduction by the F93A enzyme. It is surprising that the value of k_{-3} for the F93A enzyme is now less than the value of k_3, whereas k_{-3} for the wild-type enzyme is almost 10-fold larger than k_3 (Table 3). The rate constant for hydride transfer is proportional to the energy barriers between the Michaelis complexes (ground states for the reactions) and the transition state. Thus, the altered rate constants reflect differences in the interactions of the substrates at the active site.

The F93A substitution does not affect the overall structure of the enzyme. The major difference between the wild-type and F93A ternary complexes is in the binding of the substrates. The substitution removes the steric interactions of the phenylalanine side chain, which increases the mobility of the bound substrates. This is shown by the lack of definitive electron density for the pentafluorobenzyl alcohol in the F93A structure and the increased rate of exchange from the ^{19}F NMR experiments. Line shape analysis of the spectrum for the F93A enzyme complex suggests the pentafluorobenzyl ring is rapidly flipping, with a rate constant of about 20 000 s^{-1}. This flip rate is rather fast, but the bound alcohol now has a larger space in which to move. Solid-state deuterium NMR studies on alpha-lytic protease have found the ring flipping rates of the four tyrosines in the enzyme to vary from less than 10^3 s^{-1} to more than 10^7 s^{-1} (*50*). These studies suggest the rate constant of 20 000 s^{-1} for the rotation of the pentafluorobenzyl alcohol bound to the F93A enzyme is reasonable.

A comparison of the rates of hydride transfer and rates of pentafluorobenzyl alcohol flipping for the wild-type and F93A enzymes suggests that the increase in substrate mobility decreases the rate constant for hydride transfer. This probably reflects the ability of the enzyme to preorganize the substrates for hydride transfer. Without the phenylalanine side chain in the active site, the substrates have a decreased probability for the α-carbon to orient in the correct conformation for hydride transfer to occur. Thus, in the F93A enzyme the ensemble of bound substrate conformations is shifted toward conformations that are nonproductive for catalysis. It is surprising that the greatly increased mobility of the substrate decreases the rate constant for hydride transfer from benzyl alcohol by only 7-fold. However, the mobility of the inhibitor was determined from pentafluorobenzyl ring "flipping", and the effect of the F93A substitution on the mobility and orientation of the α-carbon was not directly determined. It is possible that the methylene group remains in a productive conformation while the pentafluorobenzyl ring rotates, but the alcohol does not appear from the X-ray results to bind in a single conformation.

The differential effects of the F93A substitution on the hydride transfer rate constants for oxidation and reduction may be due to the chemical bond structure of the alcohol and aldehyde and their differing abilities to access conformations that are productive for catalysis. While ligated to the active site zinc, the alcohol can rotate about the two single bonds of the methylene carbon (O−C7 and C7−C1) and the Zn−O bond to produce orientations favorable for hydride transfer to the C4 of the nicotinamide ring (*49*). With benzaldehyde, rotation about the double bond of the carbonyl group cannot occur, so the molecule can only rotate about the Zn−O and C7−C1 bonds, which makes the benzaldehyde less mobile. In the absence of the Phe-93 side chain, benzyl alcohol, as compared to benzaldehyde, may more readily form the correct conformation for hydride transfer. With the wild-type enzyme, the lack of flexibility with the aldehyde is counteracted by the side chain of Phe-93, which restrains the bound conformations. This can explain the 130-fold decrease in the rate constant for hydride transfer to benzaldehyde that occurs with the F93A substitution.

The studies presented here support the idea that enzymes have high catalytic efficiency when the substrates are bound in suitable orientations and that substrate mobility is a factor in the rates of catalysis. However, the differential effects of the increase in mobility on the rate constants of hydride transfer for the alcohol and aldehyde show that the relationship between substrate mobility and the rate of the chemical step is not simple. Further studies are required to provide quantitative correlations between substrate mobility and the rates of catalysis with alcohol dehydrogenase and other enzymes.

ACKNOWLEDGMENT

We thank Professor S. Ramaswamy for collecting the data for the F93A enzyme and for assistance with the X-ray crystallographic refinement, William Kearney of The University of Iowa College of Medicine Nuclear Magnetic Resonance Facility for assistance with the 1D ^{19}F-NMR spectra, John Snyder of The University of Iowa High Field Nuclear Magnetic Resonance Facility for performing the ^{19}F-^{19}F-EXSY NMR experiments, and Professor Alex Bain for assistance with the program Mexico. We also thank The University of Iowa Macromolecular Crystallography Facility and the Industrial Macromolecular Crystallography Association Collaborative Access Team (IMCA-CAT) at the Advanced Photon Source. Data were collected at beamline 17-ID in the IMCA-CAT facilities, which are supported by the companies of the Industrial Macromolecular Crystallography Association through a contract with Illinois Institute of Technology (IIT), executed through IIT's Center for Synchrotron Radiation Research and Instrumentation. Use of the Advanced Photon Source at Argonne National Laboratory was supported by the U.S. Department of Energy, Basic Energy Sciences, Office of Science, under contract No. W-31-109-Eng-38.

NOTE ADDED AFTER PRINT PUBLICATION

Because of an error, 10 μN F93A ADH and 20−240 μM benzyl alcohol in footnote a of Table 3 were published incorrectly (10 μM F93A ADH and 20−240 μN benzyl alcohol, respectively) in the version published on the Web 12/03/02 (ASAP) and in the December 31, 2002, issue (Vol. 41, No. 52, pp 15770−15779). The correct electronic version of the paper was published 01/08/03, and an Addition and Correction appears in the February 4, 2003, issue (Vol. 42, No. 4).

REFERENCES

1. Bentley, R. (1978) *Nature 276*, 673−676.
2. Jencks, W. P. (1987) *Cold Spring Harbor Symp. Quant. Biol. 52*, 65−73.
3. Wolfenden, R. (1972) *Acc. Chem. Res. 5*, 10−18.
4. Feeney, J. (2000) *Angew. Chem., Int. Ed. Engl. 39*, 290−312.
5. Nowak, T., and Mildvan, A. S. (1972) *Biochemistry 11*, 2813−2818.
6. Sanders, C. R., Tian, G., and Tsai, M. D. (1989) *Biochemistry 28*, 9028−9043.
7. Lee, H., Ortiz de Montellano, P. R., and McDermott, A. E. (1999) *Biochemistry 38*, 10808−10813.
8. Veenstra, D. L., and Gerig, J. T. (1998) *Magn. Reson. Chem. 36*, S169−S178.
9. Sylvia, L. A., and Gerig, J. T. (1993) *Biochim. Biophys. Acta 1163*, 321−334.
10. Stockman, B. J., Waldon, D. J., Gates, J. A., Scahill, T. A., Kloosterman, D. A., Mizsak, S. A., Jacobsen, E. J., Belonga, K. L., Mitchell, M. A., Mao, B., Petke, J. D., Goodman, L., Powers, E. A., Ledbetter, S. R., Kaytes, P. S., Vogeli, G., Marshall, V. P., Petzold, G. L., and Poorman, R. A. (1998) *Prot. Sci. 7*, 2281−2286.
11. Cannon, W. R., Singleton, S. F., and Benkovic, S. J. (1996) *Nat. Struct. Biol. 3*, 821−833.
12. Bruice, T. C., and Benkovic, S. J. (2000) *Biochemistry 39*, 6267−6274.
13. Luo, J., and Bruice, T. C. (2001) *J. Am. Chem. Soc. 123*, 11952−11959.
14. Lightstone F. C., and Bruice T. C. (1996) *J. Am. Chem. Soc. 118*, 2595−2605.
15. Bahnson, B. J., Park, D.-H., Kim, K., Plapp, B. V., and Klinman, J. P. (1993) *Biochemistry 32*, 5503−5507.
16. Bahnson, B. J., Colby, T. D., Chin, J. K., Goldstein, B. M., and Klinman, J. P. (1997) *Proc. Nat. Acad. Sci. U.S.A. 94*, 12797−12802.
17. Kohen, A., Cannio, R., Bartolucci, S., and Klinman, J. P. (1999) *Nature 399*, 496−499.
18. Antoniou, D., and Schwartz, S. D. (2001) *J. Phys. Chem. B 105*, 5553−5558.
19. Cui, Q., Elstner, M., and Karplus, M. (2002) *J. Phys. Chem. B 106*, 2721−2740.
20. Alhambra, C., Corchado, J., Sanchez, M. L., Garcia-Viloca, M., Gao, J., and Truhlar, D. G. (2001) *J. Phys. Chem. B 105*, 11326−11340.
21. Billeter, S. R., Webb, S. P., Agarwal, P. K., Iordanov, T., and Hammes-Schiffer, S. (2001) *J. Am. Chem. Soc. 123*, 11262−11272.
22. Rubach, J. K., Ramaswamy, S., and Plapp, B. V. (2001) *Biochemistry 40*, 12686−12694.
23. Ramaswamy, S., Eklund, H., and Plapp, B. V. (1994) *Biochemistry 33*, 5230−5237.
24. Searle, M. S., Forster, M. J., Birdsall, B., Roberts, G. C. K., Feeney, J., Cheung, H. T. A., Kompis, I., and Geddes, A. J. (1988) *Proc. Nat. Acad. Sci. U.S.A. 85*, 3787−3791.
25. Ganzhorn, A. J., and Plapp, B. V. (1988) *J. Biol. Chem. 263*, 5446−5454.
26. Kim, K., Ph.D. Thesis, The University of Iowa, 1994.
27. Park, D. H., and Plapp, B. V. (1991) *J. Biol. Chem. 266*, 13296−13302.
28. Theorell, H., and Yonetani, T. (1963) *Biochem. Z. 338*, 537−553.
29. Cleland, W. W. (1979) *Methods Enzymol. 63*, 103−138.
30. Andersson, P., and Pettersson, G. (1982) *Eur. J. Biochem. 122*, 559−568.
31. Frieden, C. (1994) *Methods Enzymol. 240*, 311−322.
32. Navaza, J. (1994) *Acta Crystallogr. 50*, 157−163.
33. CCP4 Suite (1994) *Acta Crystallogr. Sect. D, D50*, 760−763.
34. Jones, T. A., Zou, J. Y., Cowan, S. W., and Kjeldgaard, M. (1991) *Acta Crystallogr. Sect A A47*, 110−119.
35. Vriend, G. (1990) *J. Mol. Graphics 8*, 52−56.
36. Laskowski, R. A., MacArthur, M. W., Moss, D. S., and Thornton, J. M. (1993) *J. Appl. Crystallogr. 26*, 286−290.
37. Jeener, J., Meier, B. H., Bachmann, P., and Ernst, R. R. (1979) *J. Chem. Phys. 71*, 4546−4553.
38. Freeman, R., Kempsell, S. P., and Levitt, M. H. (1980) *J. Magn. Reson. 38*, 453−479.
39. Bain, A. D., and Duns, G. J. (1996) *Can. J. Chem. 74*, 819−824.
40. Sekhar, V. C., and Plapp, B. V. (1990) *Biochemistry 29*, 4289−4295.
41. Eklund, H., Samama, J. P., Wallén, L., Brändén, C.-I., Åkeson, Å., and Jones, T. A. (1981) *J. Mol. Biol. 146*, 561−587.
42. Ramaswamy, S., Scholze, M., and Plapp, B. V. (1997) *Biochemistry 36*, 3522−3527.
43. Cho, H., Ramaswamy, S., and Plapp, B. V. (1997) *Biochemistry 36*, 382−389.
44. *CRC Handbook of Chemistry and Physics* (1991) 71st ed., p 9-1, The Chemical Rubber Co., Cleveland, OH.
45. Nyburg, S. C., and Faerman, C. H. (1985) *Acta Crysallogr. B41*, 274−279.
46. Bondi, A. (1964) *J. Phys. Chem. 68*, 441−451.
47. Gerig, J. T., and Moses, J. M. (1987) *J. Chem. Soc., Chem. Commun.* 482−484.
48. Lau, E. Y., and Gerig, J. T. (2000) *J. Am. Chem. Soc. 122*, 4408−4417.
49. Eklund, H., Plapp, B. V., Samama, J. P., and Brändén, C.-I. (1982) *J. Biol. Chem. 257*, 14349−14358.
50. Burke, P. A., Griffin, R. G., and Klibanov, A. M. (1992) *J. Biol. Chem. 267*, 20057−20064.
51. Klinman, J. P. (1972) *J. Biol. Chem. 247*, 7977−7987.
52. Weidig, C. F., Halvorson, H. R., and Shore, J. D. (1977) *Biochemistry 16*, 2961−2922.
53. Dunn, M. F., Bernhard, S. A., Anderson, D., Copeland, A., Morris, R. G., and Roque, J. P. (1979) *Biochemistry 18*, 2346−2354.
54. Plapp, B. V. (1970) *J. Biol. Chem. 245*, 1727−1735.
55. Dworschack, R. T., and Plapp, B. V. (1977) *Biochemistry 16*, 2716−2725.
56. Brunger, A. T. (1992) *Nature 355*, 472−475.
57. Lian, L.-U., and Roberts, G. C. K. (1993) Effects of Chemical Exchange on NMR Spectra in *NMR of Macromolecules, A Practical Approach* (Roberts, G., Ed.) pp 153−182, Oxford Press, Oxford.
58. Johnson, M. L., and Frasier, S. G. (1985) *Methods Enzymol. 117*, 301−342.

BI026581H